Simulation of AA 6070 Recrystallization in TIG Welding

MirJavad Mirnajd Gerami[1], Eslam Ranjbarnodeh*[,1,2] , Mehdi Farajpour[1]

[1] *Lecturer, Department of Engineering, Islamic Azad University, East Tehran Branch, Tehran, Iran*
[2] *Assistant Professor, Department of Mining and Metallurgical Engineering, Amirkabir University of Technology, Tehran, Iran*

ARTICLE INFO

Article history:

Received 6 April 2017
Accepted 5 November 2018
Available online 15 March 2018

Keywords:

Heat transfer
Recrystallization
TIG welding
Aluminum 6070
Finite element method

ABSTRACT

Aluminum alloys have many applications in transportation industry because of their abundance, ease of production, and appropriate mechanical and physical properties. One of these alloys is obtained by combining aluminum with silicon and magnesium (Al-Mg-Si alloys). Since the plates of this alloy are rolled up, heat transfer and crystallization in the heat-affected zone is an important point in their welding. In this study, we have attempted to investigate welding-induced recrystallization in this alloy using the finite element method. For this purpose, the physics of the problem was defined and simulated using the ANSYS software. In the next step, the results of theoretical (simulated) and experimental investigations were compared and the effect of current on the size of weld pool and thermal cycle of different samples was assessed. Then, through microscopic examination of different areas of the welded samples, the size of recrystallized area was measured and compared with the results of mathematical calculations. Finally, the hardness of the weld zone and recrystallized area was analyzed. A temperature of 630°C and a holding time of about 0.3 s will be sufficient for recrystallization of this alloy during welding.

1-Introduction

Due to their abundance, ease of production, as well as appropriate mechanical and physical properties such as low-density, aluminum alloys have found many applications in the transportation industry. One of these alloys is produced by combining silicon and magnesium with aluminum (Al-Mg-Si alloys). These alloys are widely used in industrial structures, aerospace, automotive, and electronic industries due to such features as excellent ductility, good capability of recovery, low density, proper resistance to corrosion, moderate strength during heat treatment and suitable weldability. Heat transfer and recrystallization in the heat-affected zone (HAZ) is an important issue in the welding of this alloy by arc welding method. When the hardened material is subjected to heat treatment, the deformed metal will tend to recrystallize. With the increase of temperature and annealing duration, recrystallization will increase while strength and hardness of work hardened metal will decrease. During the welding, the impact of work hardening is completely eliminated in the welded metal due to melting and is reduced in the HAZ due to recrystallization and grain growth, and this reduced strength should be considered in the design of the welded structures. Therefore, the simulation of heat transfer and its resulting recrystallization is highly practical for welding, and several studies have been conducted in this respect. For instance, Seo et al. [1] used three-dimensional Monte Carlo simulation to study the kinetics of Zr recrystallization with a given energy storage gradient. Caleyo et al. [2]

[1] Corresponding author:
E-mail: Islam_ranjbar@aut.ac.ir

performed Monte Carlo simulation of Fe-50%Ni recrystallization. Zuñiga et al. [3] performed numerical simulation of recrystallization in BCC metals, and Zhou et al. [4] simulated recrystallization after hot deformation in low alloy steel. Medina et al. [5], as well as Abed et al. [6] reported that during rolling, dynamic recrystallization is the mechanism governing softening, which was simulated for multipass forming process. Militzer [7] studied the growth of low-carbon steel microstructure and simulated the static recrystallization in it. Zhang et al. [8] studied local boundary migration due to recrystallization in pure aluminum and showed that it is more complex than that assumed up to that time. Chekhonin et al. [9] assessed limited recrystallization in high-purity aluminum during the rolling-binding process by laboratory methods and showed that partial sporadic recrystallization occurs in high-purity layers. Saai et al. [10] assessed and compared the impact of recrystallization on aluminum plates by a numerical method. Guo et al. [11] evaluated the effect of homogenization on recrystallization behavior in 7150 aluminum sheets and showed that there will be less recrystallization with finer granules compared to the application of a single homogenization step. Yang et al. [12] assessed the impact of the strain rate on the yield stress and dynamic recrystallization mechanism in aluminum alloy (Al-Zn-Mg-Cu) during hot deformation and observed that with increasing strain rate, the required energy for discontinuous dynamic recrystallization is provided while the continuous dynamic recrystallization is delayed. Li et al. [13] studied dynamic recrystallization behavior in 7085aluminum alloy during hot deformation. Barenji [14] studied the influence of heat input on microstructural evolution during friction stir welding of pure copper. Golezani et al. [15] investigated the effect of rotational speed on microstructure and hardness of 7020-T6. Heidarzadeh et al. [16] used response surface method to predict tensile properties of friction stir welded AA 7020 aluminum alloy.

Despite these studies and to the best of our knowledge, there has been little research concerning the simulation of recrystallization during welding in aluminum alloys. Therefore, in this study, recrystallization due to welding in 6070 aluminum alloy was theoretically and experimentally investigated and the impact of current magnitude on the extent of the recrystallization area was microscopically studied.

2- Finite element simulation

In this study, a model was developed according to Fig. 1 in which the thickness, width, and length of both sides of weld joints were constant and equal to 3.5, 54 and 120 mm, respectively. SOLID70 elements were used in three-dimensional analysis of heat transfer and due to extreme temperature gradients in areas near the weld line smaller elements were used in these areas. The geometry and mesh of the model is shown in Fig. 1. Also, the analysis of SURF152 surface elements was used to apply heat flux. The thermal boundary conditions in the three-dimensional model have been shown in Fig. 2. In the finite element model, 33408 volumetric elements, 2304 surface elements, and 37583 nodes were used.

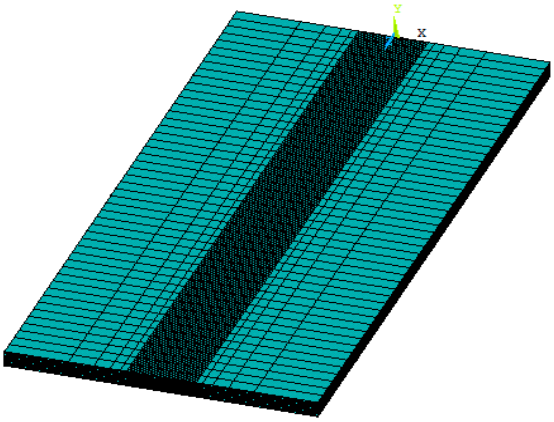

Fig.1. Generated mesh for the FE model

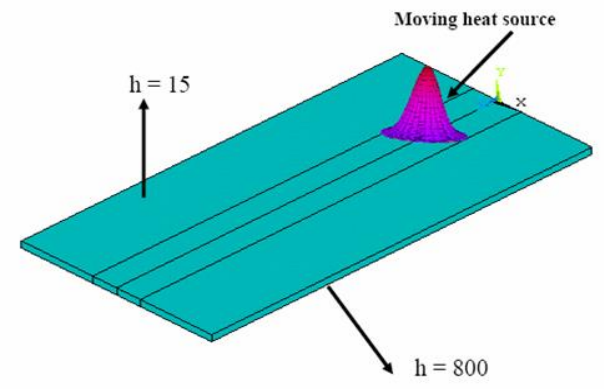

Fig. 2. Thermal boundary conditions in the three-dimensional model

The heat input of the work piece per unit time is expressed as the product of arc voltage (V) in current (I) and in efficiency of the electric arc (η) according to Eq. (1) [17]:

$$Q = \eta VI \qquad .1$$

Various resources have suggested different values for $\eta = 0.5$ to $\eta = 0.8$ [18]. The thermal energy is normally distributed on the surface and will be considered as Eq. (2):

$$q(r) = \frac{3Q}{\pi r'^2} \exp(\frac{-3r^2}{r'^2}) \qquad .2$$

Where Q is the thermal energy per unit time, r distance from the center of heat source, and rprime is the Gaussian distribution parameter. The thermal properties used in the simulation are as follows: K=225 W/mK, ρ=2710 Kg/m^3, C=891 J/Kg.C.

3- Research method

In this study, AA 6070 alloy including Al-Si-Mg alloys was used. Aluminum with a purity of 99.85% was used to produce this alloy, and the desired alloy, the chemical composition of which is shown in Table 1, was made by adding alloy elements of silicon, magnesium, manganese, and commercial pure copper. It is a 6xxx series aluminum alloy and has the highest strength of this series of aluminum alloys due to higher silicon content.

Table 1. Chemical composition of AA 6070 alloy

Si	Mg	Cu	Mn	Al
1.5	1	0.3	0.7	96.5

In this study, permanent mold casting was used to prepare the sample for the observation of microstructure and performing the next steps. A resistance furnace equipped with a K-type thermocouple with an accuracy of ±5°C and a crucible made of silicon carbide with a capacity of 30 kg of cast iron was used for alloying. The loading temperature was chosen at 750°C. After casting and obtaining the alloy ingots, the ingots were cut in smaller dimensions for remelting. The procedure was as follows: first, the small fragments of the developed alloy were molten in a silicon carbide cartridge with a capacity of 3 kilograms of cast iron using a resistance furnace of the mentioned accuracy at 750°C. Simultaneous with alloy melting, the graphitizer was preheated up to 300°C and added to the melt after removing the slag. After five minutes of brief stirring, the slag was again removed and the resulting melt was collected in the casting mold. The steel cylindrical mold was placed on a copper plate.

The samples required for rolling operations were then prepared by a crank saw from the cast ingots with 6×12×150 mm dimensions. In order to prevent any cracks on the sample surface during the rolling process, the surfaces of the cast ingots were milled by a milling machine with 0.1 surface finish. Then, the surface of the rolled samples in contact with rollers was polished using sandpaper.

In the next step, the initial plastic deformation was applied on samples. For this purpose and to increase the internal energy of the system, a hot rolling process at 400°C was used to prevent cracking of the piece. The cross-section of the prepared samples was reduced by 80% during a two-step hot rolling process. Then, TIG welding was performed on three samples to validate the simulated welding model. Fig. 3 shows the automatic welding equipment. It is worth noting that the welding operations were performed without the filler metal at a constant rate (V=3.75 mm/sec) in three different currents of 103 A, 109 A, and 120 A, respectively. EWTH-2 electrode according to AWS has been used. This type of electrode contains 2% (1.7% to 2.2%) of thoriated tungsten. Fig. 4 shows the welded samples.

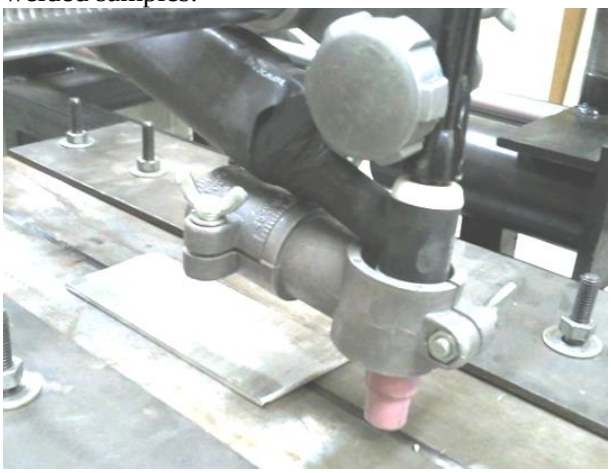

Fig. 3. Automatic TIG welding machine

Fig. 4. The welded samples

To prepare the metallography samples to be reviewed by an optical microscope, sanding operations were carried out by 120, 400, 800, 1000, 2500, 3000, and 5000 sandpapers, and Mahut cloth and 0.3μm Al_2O_3 powder were used for final polishing. The Keller solution (a mixture of 2.5% nitric acid, 1.5% hydrochloric acid and 1% hydrofluoric acid) was used for etching. The submergence time for conditions of semi-solid samples was 55-60 seconds. After preparing the surface, its structure was photographed with 100× to 400× magnification under an optical microscope equipped with an image recorder camera and Clemex version 3.5.025 software. Also, Vickers micro-hardness scale was used to measure hardness. The applied load in micro-hardeness test was 100 gf and the hardness was measured from different areas such as the welding metal, the recrystallization region, and the base metal immediately after welding and two months after the welding operations.

4- Results and discussion

Figs. 5, 6 and 7 demonstrate macro etched samples as well as analytic results. As can be seen in these figures, the overall simulated pool and experimental results are consistent with each other. For a comprehensive assessment, the width and depth of analytical and experimental results are compared, denoting acceptable differences.

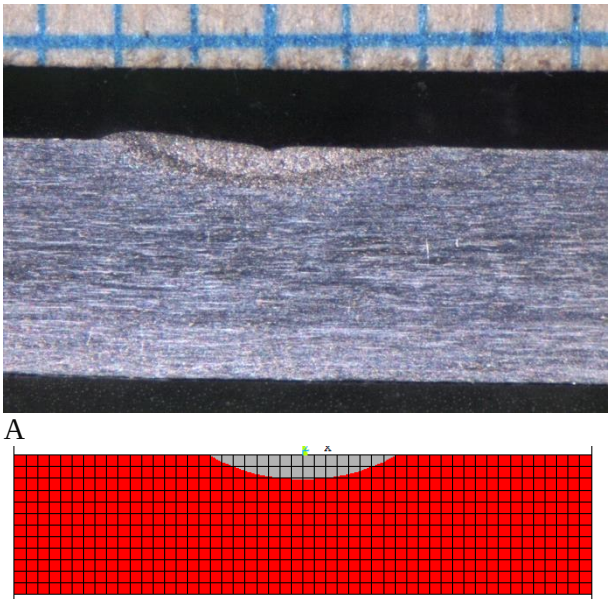

Fig. 5. The welded sample at 103 amps: a) experimental and b) simulation

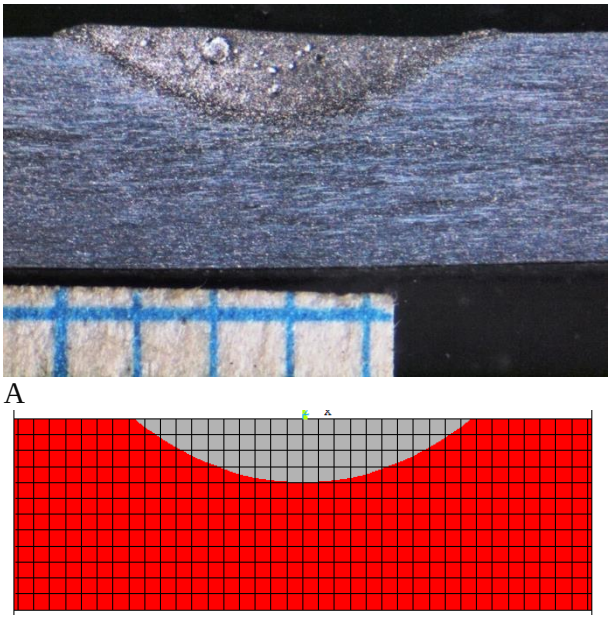

Fig. 6. The welded sample at 109 amps: a) experimental and b) simulation

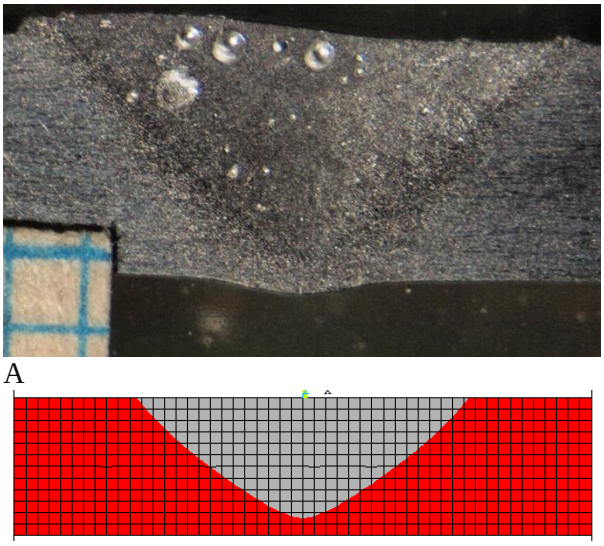

Fig. 7. The welded sample at 120 amps: a) experimental and b) simulation

Table 2. Analytical (simulated) and experimental findings for the width and depth of the weld pool

	Experimental results		Simulated results	
Sample number	D	W	D_A	W_A
1	0.35	3.1	0.5	4
2	1.21	4.85	1	5.25
3	2.84	6.58	2.63	7.25

Figs. 8 (a) and (b) show the temperature distribution at the end of welding and two minutes after its end, respectively. As can be seen, the maximum temperature at this time reaches nearly 258°C. Fig. 9 shows the effect of current on temperature distribution on the middle cross-section of the sample. According to $Q_w = \eta \frac{U_I}{V}$ equation, increased amperage increases heat input, resulting in a maximum temperature of 726°C in sample 1 (with 103 amperes), showing 20% increase versus 16% change of electric current that leads to 881°C temperature in sample 3.

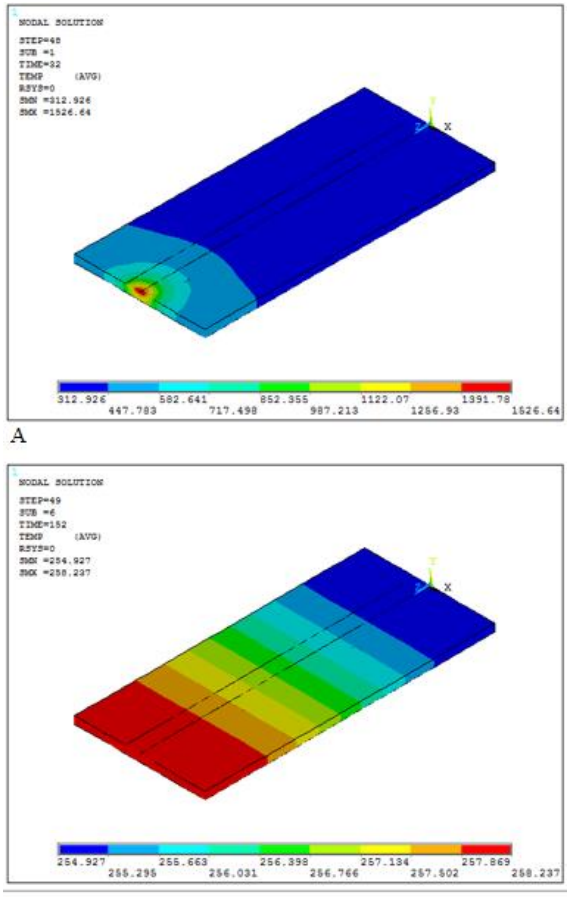

Fig. 8. Temperature distribution in the 48th step: a) at the end of welding and b) two minutes after its end

In the following, using the metallography results, the microstructure of different areas in the samples has been evaluated. According to Fig. 10, the base metal has a hard-rolled structure and the stretched structure is clearly visible.

In Fig. 11, the recrystallization area in each sample is shown. As can be seen in all these three microstructures, the structure in this area has turned into fine coaxial granules from the stretched form of the base metal.

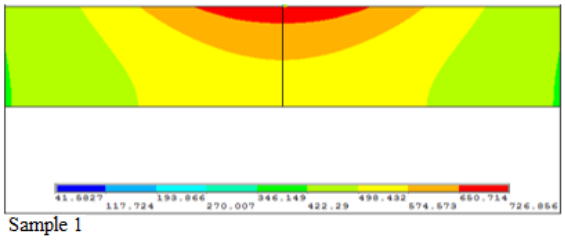
Sample 1

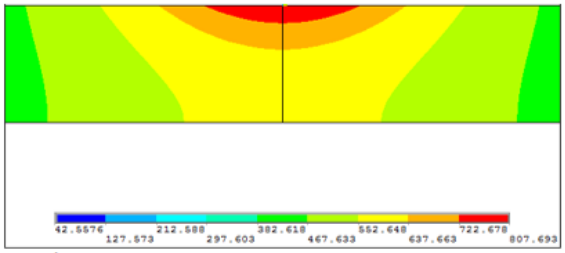
Sample 2

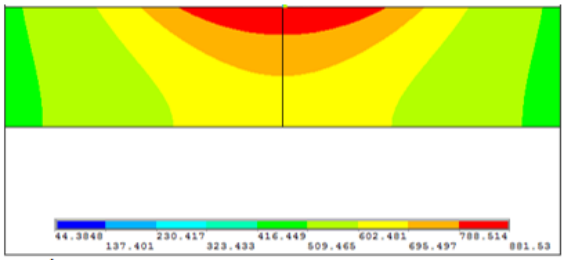
Sample 3

Fig. 9. The effect of electric current on temperature distribution in the middle cross-section of sheets, weld current: Sample 1) 103 A, Sample 2)109 A and Sample 3)120 A

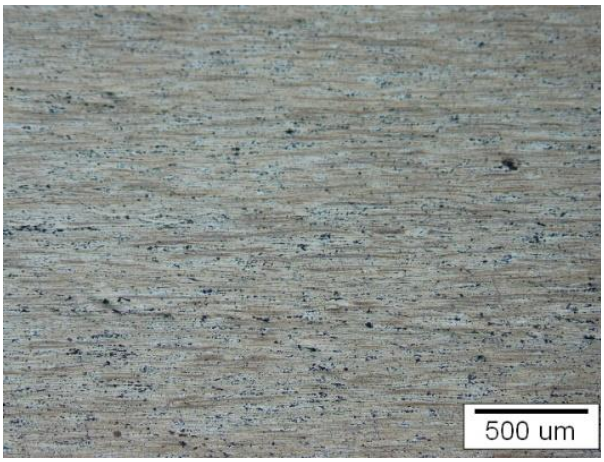

Fig. 10. The microstructure of the base rolled metal

In the welded samples, cumulative heat input caused by increased electric current has increased the width of recrystallization area as shown in Table 3.

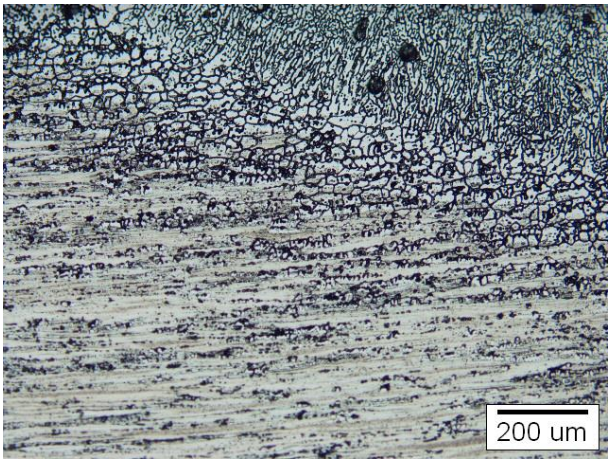

Sample 1

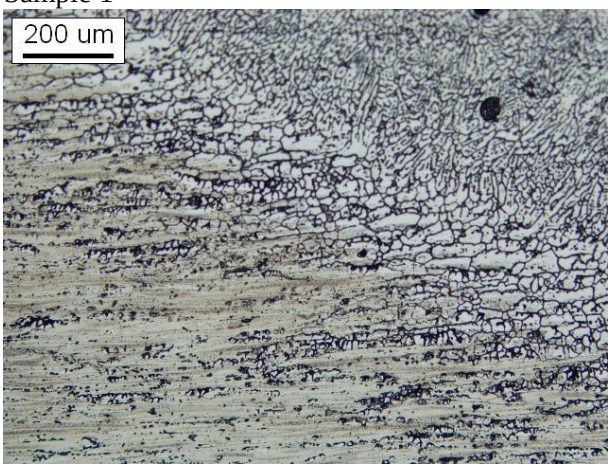

Sample 2

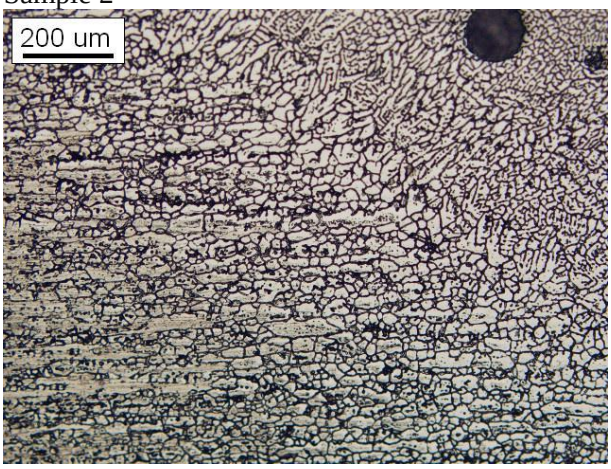

Sample 3

Fig. 11. Samples microstructure after welding, the base metal, HAZ, and recrystallized zone

Table 3. The effect of electric current on average width of the recrystallized zone

Sample	1	2	3
Average width of the recrystallization area (µm)	250	280	450

The main objective of this research is to extract an estimated temperature to predict the recrystallization during the welding of this alloy. Obviously, due to the high speed of cooling during the welding process, the classic recrystallization temperature discussed in heat treatment operations is not applicable here. Given that the thermal model has been validated, the temperature of an area with a distance of 200 microns from the melting line of sample 1 was equal to 630°C by trial and error, which is presented in Fig. 12. The shape of the recrystallized area from this method for samples 2 and 3 has been shown in Fig. 12, which has the required consistency with experimental samples in terms of overall shape and quantity.

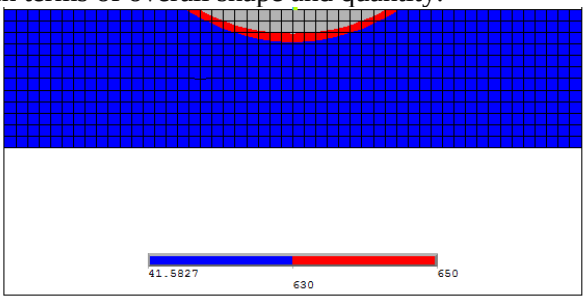

Sample 1

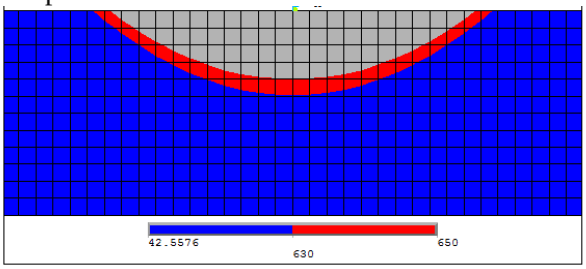

Sample 2

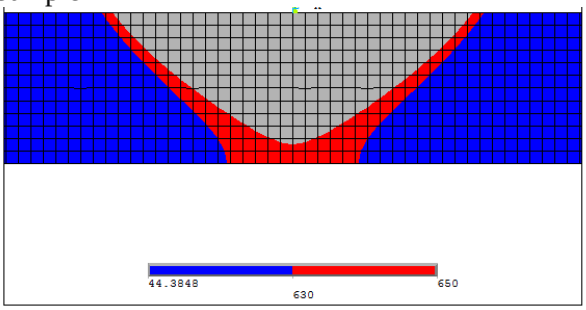

Sample 3

Fig. 12. Analytically extracted recrystallized zone

Theoretical calculations were used to re-validate this finding. Wang et al. [19] studied the effect of manganese value on recrystallization behavior of cold-rolled Al-Mg-Si-Cu alloy. One of their important findings was that manganese delays recrystallization in this alloy, increasing the activation energy of recrystallization from 134.4KJ/mol in the alloy lacking manganese to 140.1 kJ/mol in the alloy containing 0.7% manganese. We used the data of their study since the chemical composition and cold work percentage of the mentioned alloy is the same as that used in our research. Recrystallization is a process controlled with time and temperature in accordance with Eq. (3):

$$t = Ae^{(\frac{Q}{RT})} \qquad .3$$

In this paper, the time required for complete recrystallization of this alloy at 330°C has been cited as 40 minutes. Therefore, if this process should be conducted at a temperature other than 330°C, the recrystallization time would be calculated by Eq. (4):

$$\ln\frac{t_1}{t_2} = \frac{Q_r}{R}\left(\frac{1}{T_1} - \frac{1}{T_2}\right) \qquad .4$$

From equation 4 and taking into account the activation energy of 140.1 KJ/mol, the recrystallization time of 0.22 seconds is obtained. This means that if a spot in different welded areas is exposed to temperatures above 630°C during welding, then the recrystallization occurs at that spot, which has been assessed for sample 3. The temperature-time graph in recrystallization area for this sample has been presented in Fig. 13.

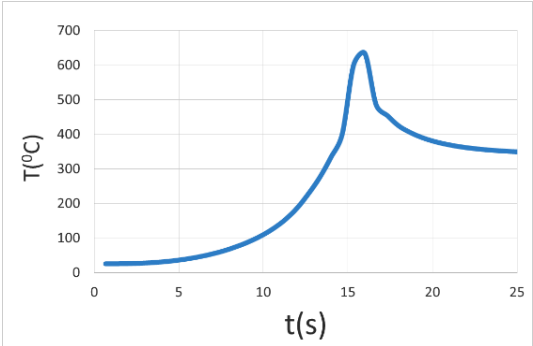

Fig. 13. Temperature-time graph in the recrystallized zone of sample 3

This point is above 630°C temperature for 0.35 seconds, which is in good agreement with 0.22 seconds. Finally, micro-hardness test results of the samples were assessed according to Table 4.

Table 4. Micro-hardness test results

Sample	Hardness value (HV)
Base metal	60
Sample 1 immediately after welding	37
Sample 1 two months after welding	71
Sample 2 immediately after welding	35
Sample 2 two months after welding	75
Sample 3 immediately after welding	36
Sample 3 two months after welding	80

The obtained hardness values immediately after welding of all samples in the recrystallization area were very close to solubilization anneal hardness value before aging of this alloy (35 Vickers), which suggests that aluminum welding has generally eliminated the effect of cold working and the high speed of cooling in welding has functioned as the solubilization operation for this area. After two months, the samples experienced normal aging and the hardness value of all of them tended towards 90, which is the hardness value of this alloy in T4 temper situation. Meanwhile, the rate of tendency towards this hardness value has been the highest for sample 3.

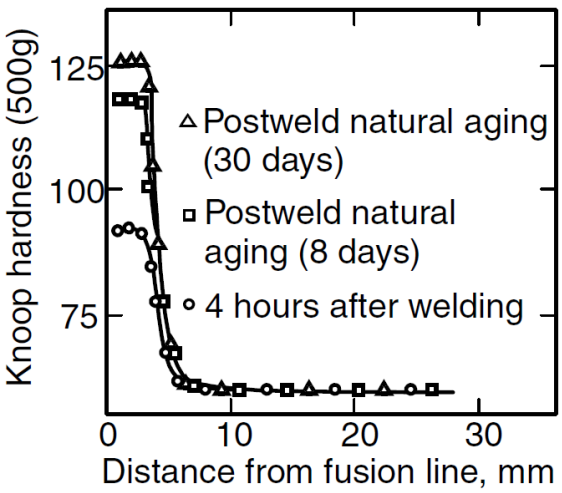

Fig. 14. HAZ hardness profiles in Al alloy welded in the annealed condition [18].

In this sample, the temperature of recrystallization areas is higher considering the increasing heat input resulting in a higher aging rate, since age hardening is a process controlled by penetration. This behavior of increasing hardness in the area affected by heat in age-hardening aluminum alloys has already been observed by researchers. An example of these observations is shown in Fig. 14.

5- Conclusion

In this study, it was attempted to assess heat transfer and recrystallization in aluminum alloy 6070 using numerical analysis and experimental study, and the main objective was determining the temperature at which recrystallization occurs. In this study, the following results were obtained:

- The developed model simulates the real sample with an acceptable error and can be used to analyze the effect of parameters on welding, as well as recrystallization area.
- An increase of 16% in electric current from 103 A to 120 A increases the maximum temperature by 20%, from 726°C to 881°C.
- In all the three welded samples, fine coaxial granular structure replaces the stretched microstructure in the rolling state.
- An increase of 16% in electric current from 103 A to 120 A widens the recrystallization area by 80%, from 250 microns in sample 1 to 450 microns in sample 3.
- The temperature at which nearly instantaneous recrystallization occurs is about 630°C for all the three samples.
- In the third sample, because of a higher electric current, the temperature of the recrystallization area is higher, thereby accelerating the aging rate.

Acknowledgement

This research was supported by Islam Azad University, East Tehran Branch.

References

[1] Y. S. Seo, Y. B. Chun, S. K. Hwang, "A 3D Monte-Carlo simulation study of

recrystallization kinetics in Zr with hypothetical stored energy gradients.", Comput. Mater. Sci, Vol. 43(3), 2008, pp. 512-521.
[2] F. Caleyo, T. Baudin, R. Penelle, "Monte Carlo simulation of recrystallization in Fe–50% Ni starting from EBSD and bulk texture measurements.", Scr. Mater., Vol. 46(12), 2002, pp. 829-835.
[3] I. M. Montaño-Zuñiga, G. Sepulveda-Cervantes, V. M. Lopez-Hirata, D. I. Rivas-Lopez, J. L. Gonzalez-Velazquez, "Numerical simulation of recrystallization in BCC metals." Comput. Mater. Sci, Vol. 49(3), 2010, pp. 512-517.
[4] J. Zhou, K. GUAN. "Deformation Resistance of Metal MI. Beijing", Mechanical Industry Press, 1988 (in Chinese).
[5] SF Medina, JE. Mancilla, "Static Recrystallization Modelling of Hot Deformed Steels Containing Severl Alloying Elements." ISIJ int., Vol. 36.8, 1996, pp. 1070-1076.
[6] R. Abad, AI Fernández, B. Lopez, JM. Rodriguez-Ibabe, "Interaction between recrystallization and precipitation during multipass rolling in a low carbon niobium microalloyed steel." ISIJ int. Vol. 41 ,2001, pp. 1373-1382.
[7] M. Militzer, "Computer Simulation of Microstructure Evolution in Low Carbon Sheet Steels", ISIJ Int., Vol.47(1), 2007, pp. 63-72
[8] Y.Zhang, A. Godfrey, D.J. Jensen, "Local boundary migration during recrystallization in pure aluminum." Scr. Mater.,Vol. 64.4 , 2011, pp. 331-334.
[9] P. Chekhonin, B. Beausir, J. Scharnweber, C. G. Oertel, T. Hausöl, H. W. Höppel, W. Skrotzki, "Confined recrystallization of high-purity aluminium during accumulative roll bonding of aluminium laminates" Acta Mater, Vol. 60(11), 2012, pp. 4661-4671.
[10] A. Saai, S. Dumoulin, O. S. Hopperstad, O. G. Lademo, "Simulation of yield surfaces for aluminium sheets with rolling and recrystallization textures.", Comput. Mater. Sci., Vol. 67, 2013, pp. 424-433.
[11] Z. Guo, G. Zhao, X. G. Chen, "Effects of homogenization treatment on recrystallization behavior of 7150 aluminum sheet during post-rolling annealing." Int J Mater Charact, Vol. 114, 2016, pp. 79-87.
[12] Q.Yang, Z. Deng, Z. Zhang, Q. Liu, Z. Jia, G. Huang, "Effects of strain rate on flow stress behavior and dynamic recrystallization mechanism of Al-Zn-Mg-Cu aluminum alloy during hot deformation.", Mater Sci Eng, A 662,2016, pp. 204-213.
[13] D. F. Li, D. Z. Zhang, S. D. Liu, Z. J. Shan, X. M. Zhang, W. A. N. G. Qin, S. Q. Han, "Dynamic recrystallization behavior of 7085 aluminum alloy during hot deformation." Transactions of Nonferrous Metals Society of China, Vol. 26.6, 2016, pp. 1491-1497.
[14] R. V. Barenji, "Influence of heat input conditions on microstructure evolution and mechanical properties of friction stir welded pure copper joints." Transactions of the Indian Institute of Metals, Vol. 69(5), 2016, pp. 1077-1085.
[15] A.S. Golezani, R.V. Barenji, A. Heidarzadeh, H. Pouraliakbar, "Elucidating of tool rotational speed in friction stir welding of 7020-T6 aluminum alloy", Int J Adv Manuf Technol, Vol. 81, 2015, pp.1155-1164.
[16] A. Heidarzadeh, R. V. Barenji, M. Esmaily, A. R. Ilkhichi, "Tensile properties of friction stir welds of AA 7020 aluminum alloy", Transactions of the Indian Institute of Metals, Vol. 68(5), 2015, pp. 757-767.
[17] A.M. Paradowska, J.W.H. Price , R. Ibrahim , T.R. Finlayson ,"The effect of heat input on residual stress distribution of steel welds measured by neutron diffraction" , J. Achieve. Mater. Manuf. Eng., Vol. 20 ,2007, pp. 319-322
[18] S. Kou, "Welding metallurgy", 2th ed., Wiley, New Jersey, 2003.
[19] Y. B. Wang, Y. Lin, J. M. Zeng, "The Effect of MN Addition on Recrystallization of Cold Rolled Al-Mg-Si-Cu Alloy". Adv. Mat. Res., Vol. 146, 2011, pp. 1874-1877.